Proceedings of The ASME 2019 Conference on Smart Materials, Adaptive Structures and Intelligent Systems
SMASIS 2019
September 9–11, 2019, Louisville, Kentucky, USA

SMASIS2019-5519

ON THE DESIGN OF A LONG-STROKE BEAM-BASED COMPLIANT MECHANISM PROVIDING QUASI-CONSTANT FORCE

Pietro Bilancia*, **Alessandro Geraci, Giovanni Berselli**
DIME - Dept. of Mechanical, Energy, Management and Transportation Engineering, University of Genova, Italy

ABSTRACT

In this paper the design of a linear long-stroke quasi-constant force compliant mechanism (CM) is presented and discussed. Starting from a flexure-based slider-crank mechanism, providing the required constant force within a rather limited deflection range, the paper reports about the shape optimization carried out with the specific aim of extending the available CM operative range. The proposed device is suitable in several precision manipulation systems, which require to maintain a constant-force at their contact interface with the manipulated object. Force regulation is generally achieved by means of complex control algorithms and related sensory apparatus, resulting in a flexible behavior but also in high costs. A valid alternative may be the use of a purposely designed CM, namely a purely mechanical system whose shape and dimensions are optimized so as to provide a force-deflection behavior characterized by zero stiffness. In the first design step, the Pseudo-Rigid Body (PRB) method is exploited to synthesize the sub-optimal compliant configuration, i.e. the one characterized by lumped compliance. Secondly, an improved design alternative is evaluated resorting to an integrated software framework, comprising Matlab and ANSYS APDL, and capable of performing non-linear structural optimizations. The new embodiment makes use of a variable thickness beam, whose shape and dimensions have been optimized so as to provide a constant reaction force in an extended range. Finally, a physical prototype of the beam-based configuration is produced and tested, experimentally validating the proposed design method.

Nomenclature

r_1	PRB model - length of the crank
r_2	PRB model - length of the connecting rod
e	PRB model - eccentricity
θ_i	PRB model - characteristic angles for $i = 1,2,3$
θ_{i0}	PRB model - initial angles for $i = 1,2,3$
T_i	PRB model - torques related to springs for $i = 1,2,3$
K_i	PRB model - torsional springs constant for $i = 1,2,3$
x	CM - slider position
x_{in}	CM - initial slider position
δ_x	CM - slider displacement along the work direction
F	CM - output force
F_t	CM - target force
e_F	CM - optimization force error
E	Material - modulus of elasticity
ν	Material - Poisson ratio
σ_{fs}	Material - flexular yield strength
b_i	CM - flexure width for $i = 1,2,3$
h_i	CM - flexure thickness for $i = 1,2,3$
L_i	CM - flexure length for $i = 1,2,3$
S_i	CM - beam reference points for $i = 1,..,6$
p_j	CM - beam design points for $j = 1,..,10$
T_i	CM - beam thickness at point S_i, for $i = 1,..,6$
t_j	CM - beam thickness at point t_j, for $j = 1,..,10$
a_j	CM - position parameter of design point p_j, for $j = 1,..,10$
B	CM - cross section width

1 INTRODUCTION

Nowadays, due to the rapid development of advanced manipulation technologies (either industrial grippers [1] or ad-

*Corresponding author
Email: pietro.bilancia@edu.unige.it

vanced anthropomorphic hands [2,3]), a precise force regulation becomes essential, especially when dealing with flexible and/or delicate objects that are particularly sensitive to the change of the contact force [4]. Robots designed to interact with humans or sensitive parts/interfaces are usually equipped with an adequate controller [5]. By using a closed loop algorithm, the manipulation force can be maintained at a specific value [6]. However, this configuration needs the presence of a precise sensory apparatus, which may be inappropriate in harsh industrial environment or in small-scale applications [7], where clearances must be accurately defined. In addition, external tactile sensors are usually very expensive. To overcome these limits, a possible solution may be the use of a constant force Compliant Mechanism (CM), which provides a reaction force at the output port that does not change for a specific range of input motion [8]. Generally speaking, also according to [9], constant force mechanisms turn useful in a large variety of applications. Besides the above-mentioned grippers, other examples may be wear testing, where a constant force should be applied to complex surfaces despite wear, or electronic connectors designed so as to maintain a constant contact reaction despite part tolerances. As for constant force mechanisms realized via the CM concept, they work trough the deflections of purposely conceived deformable members and, consequently, they do not present wear, backlash and friction, which would otherwise influence the total transmitted force [9]. Adopting a CM, a constant force output can be exerted on the manipulated part with an open loop work-cycle [10], removing the needs for force sensing and control. However, the implementation of a well designed CM would limit the force level to a single value [4,11,12] (or multiples, if mounted in parallel configuration), or to a limited range of values [7,13,14]. Another critical issue is related to fatigue life, which would limit the use of constant force CM in case of industrial high productivity scenarios.

Focusing on the recent literature in the field of linear constant force CM, the intrinsic zero-stiffness condition can be obtained resorting to two different methods [8]. The first method combines a typical positive stiffness structures, i.e. a system characterized by a directly proportionality between the applied force and the resulted displacement, with a negative stiffness structure, usually identified by a bi-stable beam [11, 15–18]. The second method refers to a single member, whose shape has to be accurately defined with the specific aim of providing a constant response. The result is a monolithic compliant solution (see [19] as an example), usually characterized by a larger available stroke. However, the complicated shape of the structure leads to possible machining error, which can affect the output force. For a more detailed review about constant force CMs, the interested reader may refer to [8]. The shape optimization has been largely used also for synthesizing constant torque CM, i.e. the rotary version of the above mentioned mechanisms. Ready examples are reported in [7,20,21].

In this paper the design of a linear long-stroke CM for robot end-effector operations, providing a quasi-constant force equalling 1.5 N, is reported. The proposed solution focuses on the well known compliant slider-crank mechanism [9]. In particular, following the classification proposed in [22], a 3A slider-crank mechanism with an additional eccentricity (i.e. an offset between the slider axis and the crank pin) has been considered in this paper, as clearly shown in Fig.1. The static of the system is initially studied using the pseudo-rigid-body (PRB) approximation [9], allowing the use of commons rigid systems analysis techniques, as the principle of virtual work. A parametric computationally efficient model has been developed in Matlab environment. By means of a fast routine, the optimal configuration, namely the correct parameter set (length of links and stiffness coefficients) allowing a specific output force, has been derived. The performance of the resulted PRB configuration is validated through RecurDyn, a commercial Multi Body Dynamics (MBD) software, also useful for CM analysis/design [23]. By replacing the spring-loaded revolute joints with equivalent small length flexural pivots (see Fig. 1), a fully compliant 3A mechanism is synthesized. The system has been analyzed by means of 1D and 3D FEA simulations, resulting in a constant force-deflection behavior available in a limited displacement range (in the order of a few mm). With the specific aim of extending the available operative stroke of the mechanism, a beam-based configuration is proposed in this paper. The new embodiment, depicted in Fig. 1, makes use of a variable thickness beam, whose shape and dimensions have been determined resorting to an integrated software framework, in which a genetic Matlab algorithm manages the optimization process, whereas ANSYS APDL is used to provide the force-deflection characteristic of each candidate. The beam-based configuration is modeled as a set of 1D tapered beams [21], numerically solved in a limited computational time. In line with the lumped compliance design, the optimal solution has been verified through a 3D FEA simulation. Finally, a physical prototype of the beam-based configuration is fabricated via

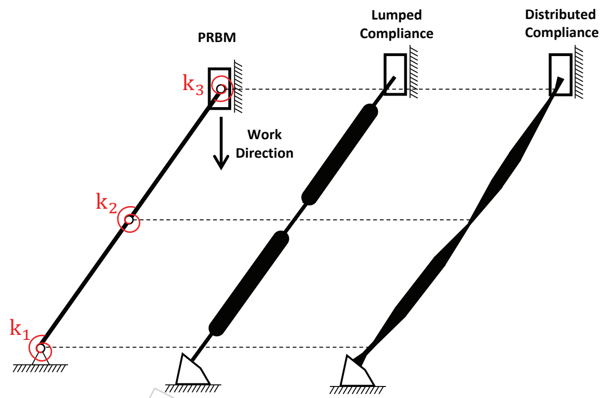

FIGURE 1. Constant force linear mechanism - PRB model and design alternatives

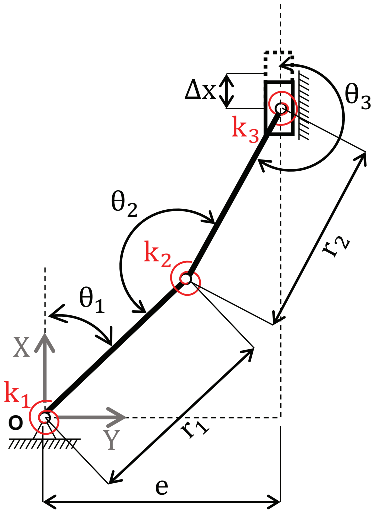

FIGURE 2. PRB model - characteristic parameters.

3D printing technology and tested by means of a special purpose test rig. The aim of the physical test is to verify the constant behavior of the mechanism as well as the absence of structural failures in the whole design stroke.
The remaining parts of the paper are organized as follows. The mechanism design is divided between sections 2 and 3. In particular, section 2 reports about the optimization study carried out on the slider crank PRB model and provides a detailed analysis of the constant force CM with lumped compliance. Afterwards, the beam-based solution as well as its design procedure are carried out in section 3. Section 4 presents the experimental activity conducted on the beam-based physical prototype. Conclusion are summarized in Section 5.

2 ECCENTRIC SLIDER MECHANISM: ANALYTICAL MODELING AND DIMENSIONAL SYNTHESIS

2.1 Optimal PRB model derivation

In this section, an analytical model for the derivation of the optimal fully compliant constant force mechanism is reported. The first design is characterized by lumped compliance. In particular, a PRB model is used to determine the stiffness of the small-length flexural pivots on the basis of a pre-defined target output force, so that the system behaves as a nonlinear compression spring. Referring to Fig. 2, r_1 and r_2 are the crank and the connecting-rod lengths respectively, e is the mechanism eccentricity, K_1, K_2, K_3 are the spring constants of the compliant joints, θ_1 and θ_3 are the crank angle and connecting rod angular position. The torques due to the presence of each spring-loaded revolute joint are given by:

$$T_i = -K_i \Psi_i \tag{1}$$

where K_i, $i = 1,2,3$ are design variables and $\Psi_1 = \theta_1 - \theta_{10}$, $\Psi_2 = \theta_2 - \theta_{20} = \theta_3 - \theta_{30} - \theta_1 + \theta_{10}$, $\Psi_3 = \theta_3 - \theta_{30}$, being θ_{10}, θ_{20} and θ_{30} the initial angles. Considering ideal frictionless joints, the static behavior of the system, i.e. the vertical output force transmitted by the slider for a given imposed Δ_x displacement, may be derived applying the principle of virtual work. From a practical standpoint, θ_1 is considered as kinematic input instead of Δ_x in this paper. By defining $\alpha = atan(\frac{e}{x})$, where x is the slider position along the working direction with respect to the fixed coordinate system, and thanks to the superposition principle, the total output force may be written as:

$$F = F_1 + F_2 + F_3 \tag{2}$$

where

$$F_1 = K_1 \Psi_1 cos(\theta_3) \Big/ r_1 sin(\theta_3 - \theta_1) \tag{3}$$
$$F_2 = K_2 \Psi_2 cos(\alpha) \Big/ r_1 sin(\theta_1 - \alpha) \tag{4}$$
$$F_3 = K_3 \Psi_3 cos(\theta_1) \Big/ x\, sin(\theta_1) - e\, cos(\theta_1) \tag{5}$$

are the contributes related to each single rotational spring. While the values of e, r_1, r_2 and θ_1 have to be considered as input, an analytical expression for x and θ_3 must be derived for computing F. From a position analysis, the following relations yield:

$$\vartheta_3 = \pi - asin\left(\frac{r_1 sin(\theta_1) - e}{r_2}\right) \tag{6}$$
$$x = r_1 cos(\theta_1) - r_2 cos(\theta_3) \tag{7}$$

Once defined the analytical formulation, a fast numerical routine aiming at providing a PRB model which exhibits a specific constant output force (equal to 1.5 N) over a range of displacements, has been set up in Matlab. Assuming r_1, θ_{10}, K_1, K_2 and K_3 as a design variables, the optimization problem can be formulated as follow:

$$\textbf{Minimize}\ \ e_F = e_F(r_1, \theta_{10}, K_1, K_2, K_3) = \\ = \sqrt{\tfrac{1}{Q}\textstyle\sum_{i=1}^{Q}\left[F - F_t\right]^2} \tag{8}$$

$$\textbf{DesignVariables} \rightarrow \begin{cases} r_1 \in [r_{1,min}, r_{1,max}] \\ \theta_{10} \in [\theta_{10,min}, \theta_{10,max}] \\ K_1 \in [K_{1,min}, K_{1,max}] \\ K_2 \in [K_{2,min}, K_{2,max}] \\ K_3 \in [K_{3,min}, K_{3,max}] \end{cases} \tag{9}$$

$$\textbf{Fixed Parameters} \rightarrow \begin{cases} x_{in} = 100\ mm \\ y_{in} = e = 60\ mm \end{cases} \tag{10}$$

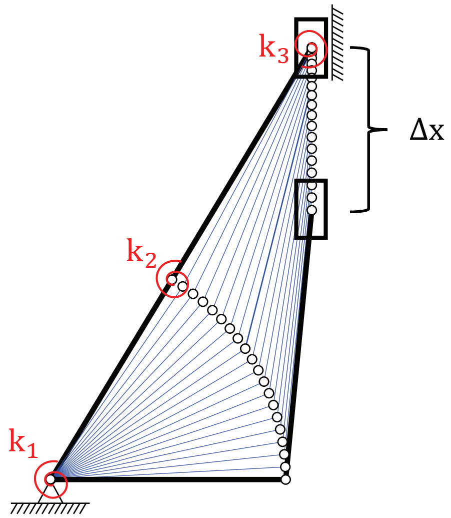

FIGURE 3. PRB model - Static analysis at different slider positions

Design Variable	Range	Opt. Value
r_1	$[e/5, (9/10)e]$ mm	54.000 mm
θ_{10}	$[asin\left(\frac{e}{\sqrt{e^2+x_{in}^2}}\right), \pi/2]$ rad	0.542 rad
K_1	$[0, 1000]$ Nmm	28.303 Nmm
K_2	$[0, 1000]$ Nmm	35.379 Nmm
K_3	$[0, 1000]$ Nmm	35.379 Nmm

TABLE 1. Optimal PRB model - characteristic parameters.

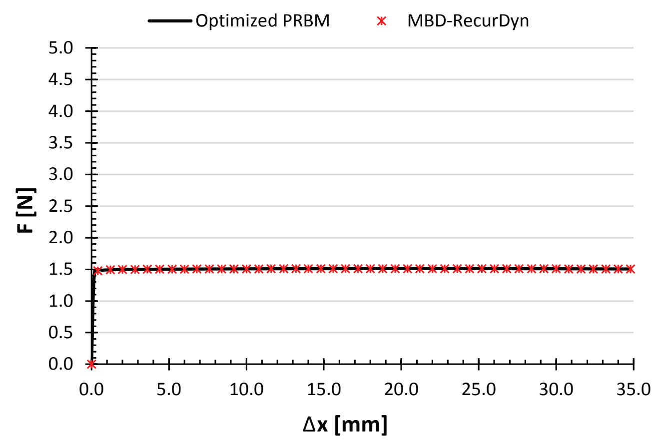

FIGURE 4. Optimal PRB model - force-deflection behavior

where e_F represents the root mean square value of the error evaluated for a single candidate in a series of Q simulation steps, namely the difference between the desired force $F_t = 1.5$ N and the force derived at each vertical position of the slider by means of the Eq. 2. A "For" loop structure with a total number of Q increments on the input variable θ_1 has been exploited for analyzing the whole linear stroke, $\Delta_x = 35$ mm, as shown in Fig. 3. The value of r_2 is simply obtained for each candidate by knowing r_1 and by considering an initial stretched configuration of the PRB model, in which the slider is placed at the coordinates (x_{in}, e) with respect to the crank pin:

$$r_2 = \sqrt{x_{in}^2 + e^2} - r_1 \tag{11}$$

The Optimal parameter set is summarized in Tab. 1, whereas the related force-deflection characteristic is reported in Fig. 4 for $Q = 100$ discrete points. In particular, Fig. 4 shows a comparison between results achieved during the optimization routine (carried out in Matlab resorting to a computationally efficient *fmnincon* command) and a final MBD simulation performed in RecurDyn for validation purpose. The plot highlights a precise matching between the PRB behavior and the target force in the whole operative range.

2.2 Flexural hinges evaluation

From the values of K_i, $i = 1,2,3$ listed in Tab. 1, the dimensions of the small length flexural pivots can be calculated. Supposing the flexures are straight beam hinges with rectangular cross section, the following relation yields:

$$K_i = \frac{EI_{a_i}}{L_i} \tag{12}$$

where E is the material modulus of elasticity, L_i is the length of the small-length flexural pivot, and $I_{a_i} = \frac{{h_i}^3 b_i}{12}$ is the moment of inertia of the pivot cross sectional area with respect to the axis a_i (h_i and b_i denotes the pivot thickness and width respectively, whereas a_i is the barycentric axis parallel to the width). The adopted material for the constant force CM is ABS plastic that has a flexural yield strength of $\sigma_{fs} = 42.5$ MPa, modulus of elasticity of $E = 1800$ MPa, and Poisson's ratio of $\nu = 0.35$ [24]. Starting from the PRB model and assuming the bending as predominant loading, the flexure dimensions have been determined considering that the PRB rigid pairs are located at the center of the related small length flexural pivots [9]. The synthesized CM is reported in Fig. 5, whereas the flexure hinges dimensions are reported in Tab. 2.

The resulted lumped compliance configuration of the constant force mechanism has been numerically analyzed via 1D and 3D non-linear (NLGEOM option) FEA simulations in ANSYS en-

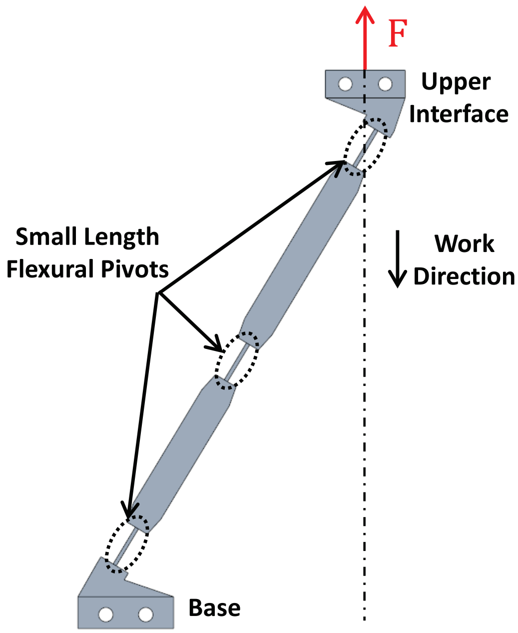

FIGURE 5. Optimal lumped compliance constant force mechanism

Dimension	b_i (mm)	h_i (mm)	L_i (mm)
Joint K_1	2.478	0.908	10.800
Joint K_2	2.621	0.960	10.800
Joint K_3	2.621	0.960	10.800

TABLE 2. Flexure dimensions.

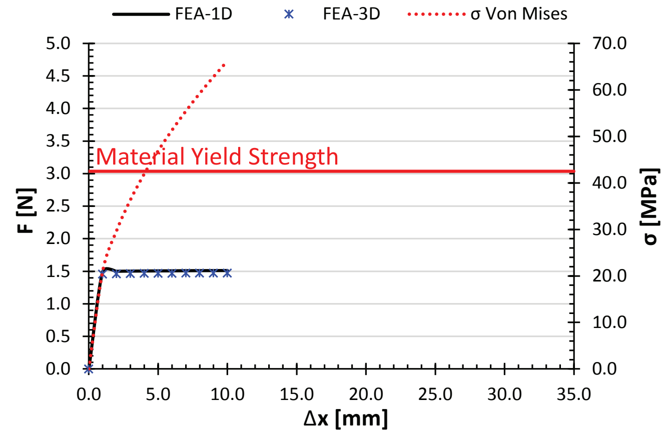

(a) Force-displacement behavior.

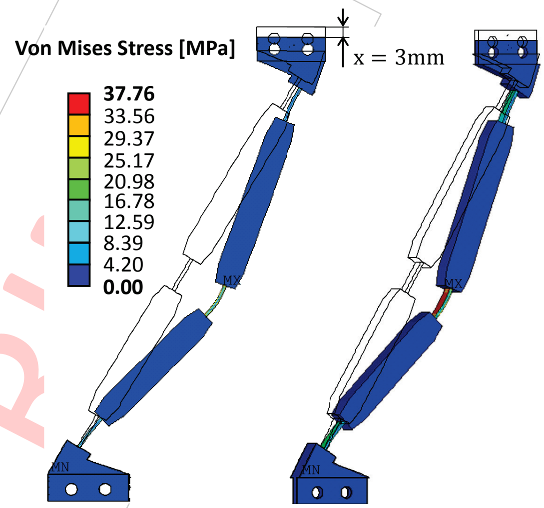

(b) Stress field at maximum available stroke.

FIGURE 6. Optimal results on the small length configuration.

vironment. Regarding the FEM models, beam 3 elements are used for the 1D analysis, whereas a free Hexa-dominant mesh has been defined (0.5 mm as max element size on the flexural hinges) for the 3D analysis. As for the B.C., the base of the system is fixed to the ground and the upper interface is guided along x direction and constrained along y direction (see Fig. 5). The FEA results are shown in Figs. 6(a)-6(b), where both the force-deflection characteristic and the 3D stress field are reported. As clearly depicted in Fig. 6(a), both the 1D and 3D FEA output show good agreement with the behavior predicted by the PRBM, even if the assessed stress field limits the use of the lumped compliance configuration to a limited linear stroke (3 mm$< \Delta_x < 4$ mm).

3 BEAM-BASED SOLUTION: A CAE SHAPE OPTIMIZATION

Focusing on the need to extend the operative stroke Δ_x of the proposed constant force CM (limited to about 3 mm in the previous design), this section reports about a shape optimization process carried out by means of an integrated software framework. The parameter optimization is conducted in this paper by using a Matlab genetic algorithm, which is particularly suitable for studies where the multi-parameters design space is not well known. In particular, thanks to the ANSYS APDL interfacing capabilities, an integrated design environment in which Matlab manages the optimization process and the data exchange activities has been implemented [25]. The performance of the CM are evaluated via a series of batch 1D non-linear FEA simulations. From a design standpoint, the idea is to maintain the general architecture of the lumped compliance design, while trying to smooth the beam's shape where the cross section undergoes remarkable variations, as shown in Fig. 7(a). In this way, the deflection would not be constricted in small areas, allowing a minor stress concentration and a major linear displacement Δ_x.

The geometrical correlation between the lumped compliance solution and the beam-based solution is clearly highlighted in Fig. 7(a). The coordinates of points S_i, $i = 1,..,6$, which represent the start/end location of each flexural hinge, are taken as a reference for designing the beam-based CM. The new embodiment makes use of linearly variable thickness segments, whose extremities are defined by design points p_j, $j = 1,..,10$ (except for the initial/final segments, which are connected also to S_1 and S_6 respectively). Each design (red) point, p_j, identifies a parametric cross section of the CM and is located at a precise distance from the closest inferior reference (blue) point S_i. Taking as an example the design point p_1, its position in the work-space can be defined as follow:

$$p_1 \rightarrow \begin{cases} x_{p_1} = x_{S_1} + a_1(x_{S_2} - x_{S_1}) \\ y_{p_1} = y_{S_1} + a_1(y_{S_2} - y_{S_1}) \end{cases} \quad (13)$$

where a_1 is the position coefficient taken into account during the optimization, along with the cross section width B_1 and thickness t_1 (having considered a rectangular section) related to the point p_1. In summary, by imposing an equal width B for all the segments of the CM, the design variables vector may be composed of 23 entities, i.e.:

- a_j, $j = 1,..,10$ (design points location);
- t_j, $j = 1,..,10$ (thickness at p_j);
- T_1, T_6 (thickness at CM's extremities, i.e. S_1 and S_6);
- B; (CM's out-of-plane width).

At each iteration of the process, the genetic algorithm updates the design variables vector, which is then included into an external "par.dat" file. The optimization problem may be formalized as follow:

$$\textbf{Minimize} \;\; e_F = e_F(a_j, t_j, T_1, T_6, B, j = 1,..,10) = \\ = \sqrt{\tfrac{1}{r}\textstyle\sum_{i=1}^{r}\left[F_{FEA} - F_t\right]^2} \quad (14)$$

$$\textbf{Constraint} \rightarrow \;\; \sigma \leq \sigma_{fs} = 42.5MPa \quad (15)$$

$$\textbf{Design Variables} \rightarrow \begin{cases} a_j \in [a_{j,min}, a_{j,max}] \; j = 1,..,10 \\ t_j \in [t_{j,min}, t_{j,max}] \; j = 1,..,10 \\ T_1 \in [T_{1,min}, T_{1,max}] \\ T_6 \in [T_{6,min}, T_{6,max}] \\ B \in [B_{min}, B_{max}] \end{cases} \quad (16)$$

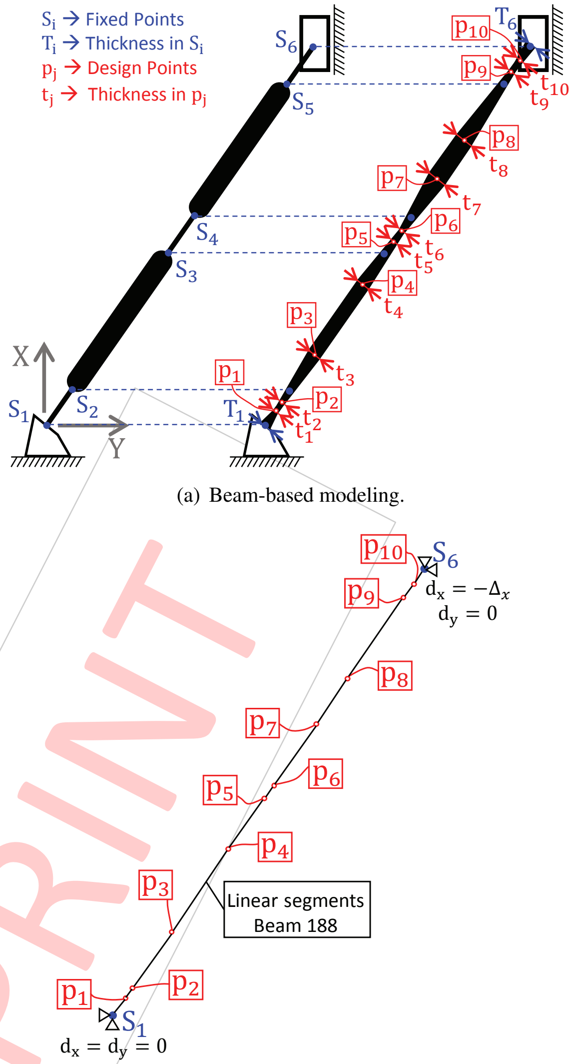

(a) Beam-based modeling.

(b) Parametric 1D FEM model.

FIGURE 7. Shape optimization parameters.

$$\textbf{Fixed Parameters} \rightarrow \begin{cases} S_{1,x} = 0.000\;mm \\ S_{1,y} = 0.000\;mm \\ S_{2,x} = 8.730\;mm \\ S_{2,y} = 6.358\;mm \\ S_{3,x} = 43.637\;mm \\ S_{3,y} = 31.779\;mm \\ S_{4,x} = 52.854\;mm \\ S_{4,y} = 37.408\;mm \\ S_{5,x} = 99.100\;mm \\ S_{5,y} = 60.746\;mm \\ S_{6,x} = 108.742\;mm \\ S_{6,y} = 65.612\;mm \end{cases} \quad (17)$$

where F_{FEA} is the output force evaluated in a series of r FEA simulation sub-steps (imposed equal to 10 in this work). The parametric FEM model, depicted in Fig. 7(b), is automatically launched from Matlab by means of a dos command. All the segments are discretized by beam 188 elements, that allow tapered cross sections. The first node (i.e. the one related to S_1) is fixed to the ground, whereas the upper node (i.e. the one related to S_6) is guided by a remote displacement $\Delta_x = 30mm$ along the work direction and constrained along the y-direction, as visible in Fig. 7(b). The APDL script is linked to the parameters "par.dat" file and provides, as a response of each non-linear FEA simulation, the force-deflection behavior of the CM as well as the maximum occurred stress. These outputs are then stored into another external "out.dat" file, which is then automatically imported and elaborated from Matlab, allowing the evaluation of the error e_F. Imposed range of variation for each parameter and optimal values are summarized in Tabs 3, whereas the final configuration is shown in Fig. 8. In line with the lumped compliance solution, a final 3D FEA simulation has been performed on the optimal beam-based configuration. The achieved results are shown in Fig. 9. In Fig. 9(a), it is possible to see the matching between the desired target force (i.e. 1.5 N), the characteristic obtained by means of the proposed design procedure (i.e. FEA-1D) and the one resulted from the last simulation (i.e. FEA-3D). The available operative linear stroke has been increased from 3 mm to 18 mm, as it can be noted from Figs. 9(a)-9(b). It must be remarked that the optimal beam-based design can be modified in case of a different target force by acting on the value of B.

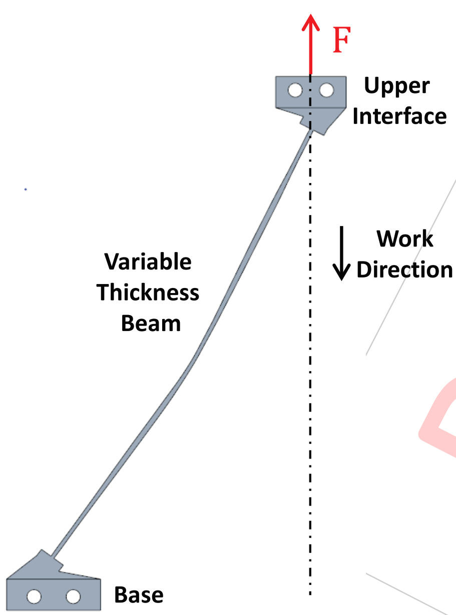

FIGURE 8. Optimal distributed compliance constant force mechanism

Design Variable	Range	Opt. Value
a_1	$[0.125, 0.500]$	0.285
a_2	$[0.625, 0.875]$	0.803
a_3	$[0.500, 0.625]$	0.582
a_4	$[0.750, 0.875]$	0.851
a_5	$[0.125, 0.375]$	0.245
a_6	$[0.625, 0.875]$	0.842
a_7	$[0.375, 0.625]$	0.578
a_8	$[0.750, 0.875]$	0.798
a_9	$[0.125, 0.375]$	0.231
a_{10}	$[0.750, 0.875]$	0.765
t_1	$[0.850, 1.100]$ mm	0.997 mm
t_2	$[0.850, 1.100]$ mm	0.929 mm
t_3	$[1.200, 1.400]$ mm	1.356 mm
t_4	$[1.200, 1.400]$ mm	1.339 mm
t_5	$[0.800, 1.150]$ mm	0.996 mm
t_6	$[0.800, 1.150]$ mm	0.920 mm
t_7	$[1.300, 1.600]$ mm	1.440 mm
t_8	$[1.300, 1.600]$ mm	1.434 mm
t_9	$[0.900, 1.100]$ mm	0.968 mm
t_{10}	$[0.900, 1.100]$ mm	1.046 mm
T_1	$[0.850, 1.100]$ mm	0.927 mm
T_6	$[0.900, 1.100]$ mm	0.947 mm
B	$[5.000, 8.000]$ mm	5.138 mm

TABLE 3. Optimal beam-based CM parameters.

4 PHYSICAL PROTOTYPING AND EXPERIMENTAL TESTS

As final step, the synthesized constant force beam-based CM has been fabricated via 3D printing (fused deposition modeling) techniques by employing a 3D printer able to extrude ABS with a layer height of 0.100 mm. Then, an experimental test has been carried out on the CM resorting to a purposely designed test rig. The test aims at verifying output force of the prototype and the absence of failures for a linear stroke equal to $\Delta_x = 18$ mm. The experimental setup, shown in Fig. 10, is equipped with a linear motor (LinMot PS02-23x80-F), a 1-axis load cell (characterized by a structural stiffness of 242.000 N/mm, an overall weight of 11 g and an accuracy of 0.1 N), and a series of 3D printed connection members. Two specimens are tested simultaneously in order to ensure the symmetry and to exclude undesired disturbance forces (e.g. friction or other out-of-axis contributes). Furthermore, the considered configuration (a couple of parallel

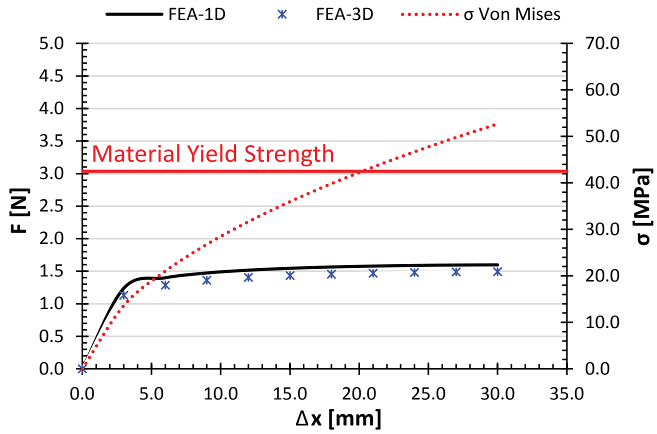

(a) Force-displacement behavior.

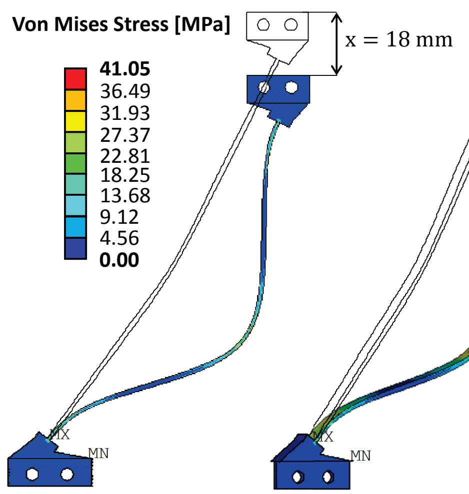

(b) Stress field at maximum available stroke.

FIGURE 9. Optimal results on the beam-based configuration.

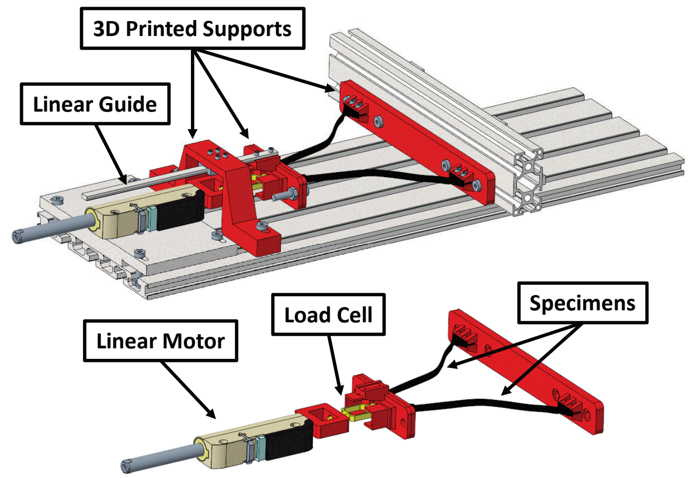

FIGURE 10. Custom experimental setup

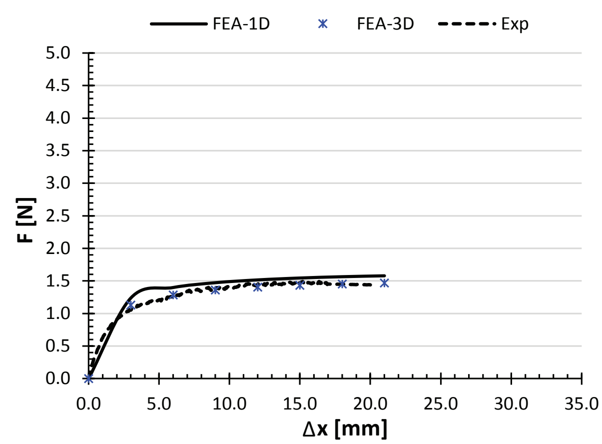

FIGURE 11. Experimental results - force-displacement behavior

springs) may be considered as an effective way to implement the proposed concept in the robot end-effector. The specimens are fixed to the ground from one end and guided in a linear motion by means of the LinMot slider on the other end. The 1-axis load cell is mounted on the LinMot slider and provides the reaction force (as a sum of both beams) at each step of the motion. A general-purpose NI-cRIO is used to acquire the data from the LinMot integrated linear encoder and the load cell. With the aim of investigating the static behavior of the system, a velocity of 2 mm/s has been assigned to the slider, neglecting the major dynamic contributes. As depicted in Fig. 11, which reports the contribute of a single beam, the experimental results show good agreement with the behavior predicted during the design step. The slight differences between FEA and experimental results are mainly due to:

- manufacturing errors in the deposition of the filament, causing uncertainties in the effective obtained thickness along the path of the beam;
- non perfectly frictionless linear guide (see Fig. 10);
- limited and tolerable misalignment in the test rig.

However, the tested specimens attest the operative linear range (i.e. $\Delta_x = 18$ mm) without structural failures, which overcome at $\Delta_x = 22$ mm.

5 CONCLUSIONS

The design of a linear monolithic CM providing quasi constant force, to be used in manipulation systems, is presented in this paper. Starting from the modeling of an eccentric crank-slider mechanism, a multi-step design procedure has been carried out with the aim of increasing the available stroke, namely the interval in which the CM provides a nearly constant output force without manifesting irreversible structural damages. In the first proposed design, characterized by lumped compliance, a fast optimization routine is performed on the equivalent PRB model in order to synthesize the small length pivots. FEA results fully verified the validity of the solution, even if highlight a critical stress condition after a limited linear displacement. The second design, characterized by distributed compliance, is obtained after a shape optimization process performed in a multi-software environment. A Matlab genetic algorithm is used to select each multi-parameter input vector, whereas ANSYS APDL is exploited to provide the force-deflection characteristic of each candidate. The resulted configuration is composed of a series of variable thickness flexible segments, which allow a better distribution of the stress and a remarkable increment (approximately 600%) of the operative stroke. The beam-based CM is then manufactured by means of 3D printing technologies and experimentally verified. The acquired data show a good consistency with the numerical results, confirming the suitability of the proposed design approach.

6 ACKNOWLEDGEMENT

The research has received funding from University of Genova grant - COSMET, COmpliant Mechanisms for MEdical Technologies.

REFERENCES

[1] Birglen, L., and Schlicht, T., 2018. "A statistical review of industrial robotic grippers". *Robotics and Computer-Integrated Manufacturing,* ***49***, pp. 88 – 97.

[2] Xiong, C., Chen, W., Sun, B., Liu, M., Yue, S., and Chen, W., 2016. "Design and implementation of an anthropomorphic hand for replicating human grasping functions". *IEEE Transactions on Robotics,* ***32***(3), pp. 652–671.

[3] Berselli, G., Guerra, A., Vassura, G., and Andrisano, A., 2014. "An engineering method for comparing selectively compliant joints in robotic structures". *IEEE/ASME Transactions on Mechatronics,* ***19***(6), pp. 1882–1895.

[4] Liu, Y., and Xu, Q., 2017. "Design of a 3D-printed polymeric compliant constant-force buffering gripping mechanism". *IEEE ICRA International Conference on Robotics and Automation*, pp. 6706–6711.

[5] Fryman, J., and Matthias, B., 2012. "Safety of industrial robots: From conventional to collaborative applications". *7th ROBOTIK German Conference on Robotics*, pp. 1–5.

[6] Wang, J.-Y., and Lan, C.-C., 2014. "A constant-force compliant gripper for handling objects of various sizes". *Journal of Mechanical Design,* ***136***(7), p. 071008.

[7] Lan, C.-C., and Wang, J.-Y., 2011. "Design of adjustable constant-force forceps for robot-assisted surgical manipulation". *IEEE ICRA International Conference on Robotics and Automation*, pp. 386–391.

[8] Wang, P., and Xu, Q., 2018. "Design and modeling of constant-force mechanisms: A survey". *Mechanism and Machine Theory,* ***119***, pp. 1–21.

[9] Howell, L. L., 2001. *Compliant mechanisms*. John Wiley & Sons.

[10] Weight, B. L., Magleby, S. P., and Howell, L. L., 2002. "Selection of compliant constant-force mechanisms based on stress and force criteria". *ASME IDETC-CIE International Design Engineering Technical Conferences and Computers and Information in Engineering Conference*, pp. 51–63.

[11] Xu, Q., 2015. "Design of a constant-force flexure micropositioning stage with long stroke". *ASME IDETC-CIE International Design Engineering Technical Conferences and Computers and Information in Engineering Conference*, pp. V05AT08A012–V05AT08A012.

[12] Liu, Y., and Xu, Q., 2016. "Design of a compliant constant force gripper mechanism based on buckled fixed-guided beam". *IEEE MARSS International Conference on Manipulation, Automation and Robotics at Small Scales*, pp. 1–6.

[13] Chen, Y.-H., and Lan, C.-C., 2012. "An adjustable constant-force mechanism for adaptive end-effector operations". *Journal of Mechanical Design,* ***134***(3), p. 031005.

[14] Tolman, K. A., Merriam, E. G., and Howell, L. L., 2016. "Compliant constant-force linear-motion mechanism". *Mechanism and Machine Theory,* ***106***, pp. 68–79.

[15] Liu, Y., Zhang, Y., and Xu, Q., 2017. "Design and control of a novel compliant constant-force gripper based on buckled fixed-guided beams". *IEEE/ASME Transactions on Mechatronics,* ***22***(1), Feb, pp. 476–486.

[16] Liu, Y., and Xu, Q., 2016. "Design and analysis of a micro-gripper with constant force mechanism". *12th WCICA World Congress on Intelligent Control and Automation*, pp. 2142–2147.

[17] Hao, G., Mullins, J., and Cronin, K., 2017. "Simplified modelling and development of a bi-directionally adjustable constant-force compliant gripper". *Proceedings of the Institution of Mechanical Engineers, Part C: Journal of Mechanical Engineering Science,* ***231***(11), pp. 2110–2123.

[18] Zhang, X., Wang, G., and Xu, Q., 2018. "Design, analysis and testing of a new compliant compound constant-force mechanism". *Actuators,* ***7***(4), p. 65.

[19] Lan, C.-C., Wang, J.-H., and Chen, Y.-H., 2010. "A compliant constant-force mechanism for adaptive robot end-effector operations". *IEEE ICRA International Conference on Robotics and Automation*, pp. 2131–2136.

[20] Hou, C.-W., and Lan, C.-C., 2013. "Functional joint mechanisms with constant-torque outputs". *Mechanism and Machine Theory,* ***62***, pp. 166–181.

[21] Prakashah, H. N., and Zhou, H., 2016. "Synthesis of constant torque compliant mechanisms". *Journal of Mecha-*

nisms and Robotics, ***8***(6), p. 064503.

[22] Weight, B. L., Magleby, S. P., and Howell, L. L., 2002. "Selection of compliant constant-force mechanisms based on stress and force criteria". *ASME IDETC-CIE International Design Engineering Technical Conferences and Computers and Information in Engineering Conference*, pp. 51–63.

[23] Bilancia, P., Berselli, G., Bruzzone, L., and Fanghella, P., 2019. "A CAD/CAE integration framework for analyzing and designing spatial compliant mechanisms via pseudo-rigid-body methods". *Robotics and Computer-Integrated Manufacturing,* ***56***, pp. 287–302.

[24] Bilancia, P., Berselli, G., Scarcia, U., and Palli, G., 2018. "Design of a beam-based variable stiffness actuator via shape optimization in a CAD/CAE environment". *ASME SMASIS Conference on Smart Materials, Adaptive Structures and Intelligent Systems*, pp. V001T03A013–V001T03A013.

[25] Gauchía, A., Boada, B., Boada, M., and Díaz, V., 2014. "Integration of matlab and ansys for advanced analysis of vehicle structures". *MATLAB Applications for the Practical Engineer*.